Dirac fermions with plaquette interactions. I. SU(2) phase diagram with Gross-Neveu and deconfined quantum criticalities

Yuan Da Liao [1,2] Xiao Yan Xu,[3] Zi Yang Meng,[4,*] and Yang Qi[1,2,5,†]

[1]*State Key Laboratory of Surface Physics, Fudan University, Shanghai 200438, China*
[2]*Center for Field Theory and Particle Physics, Department of Physics, Fudan University, Shanghai 200433, China*
[3]*Key Laboratory of Artificial Structures and Quantum Control (Ministry of Education), School of Physics and Astronomy, Shanghai Jiao Tong University, Shanghai 200240, China*
[4]*Department of Physics and HKU-UCAS Joint Institute of Theoretical and Computational Physics, The University of Hong Kong, Pokfulam Road, Hong Kong SAR, China*
[5]*Collaborative Innovation Center of Advanced Microstructures, Nanjing 210093, China*

(Received 17 April 2022; revised 7 June 2022; accepted 25 July 2022; published 4 August 2022)

We investigate the ground state phase diagram of an extended Hubbard model with a π-flux hopping term at half filling on a square lattice, with unbiased large-scale auxiliary-field quantum Monte Carlo simulations. As a function of interaction strength, there emerges an intermediate phase which realizes two interaction-driven quantum critical points, with the first between the Dirac semimetal and an insulating phase of weak valence bond solid (VBS) order, and the second separating the VBS order and an antiferromagnetic insulating phase. These intriguing quantum critical points are respectively bestowed with Gross-Neveu and deconfined quantum criticalities, and the critical exponents $\eta_{\mathrm{VBS}} = 0.6(1)$ and $\eta_{\mathrm{AFM}} = 0.58(3)$ at a deconfined quantum critical point satisfy the conformal field theory bootstrap bound. We also investigate the dynamical properties of the spin excitation and find the spin gap open near the first transition and closed at the second. The relevance of our findings in realizing deconfined quantum criticality in fermion systems and the implication to lattice models with further extended interactions such as those in quantum moiré systems, are discussed.

DOI: 10.1103/PhysRevB.106.075111

I. INTRODUCTION

The Landau-Ginzburg-Wilson (LGW) paradigm of phases and their transitions is one of the cornerstones of modern condensed matter physics [1,2], in which the phase transition could be understood in terms of symmetry breaking and the establishment of order parameters. According to LGW, the transition between two ordered phases with spontaneously broken symmetries should either be first order or through an intermediate phase. However, new transitions between novel quantum states that are beyond the LGW have been accumulating in recent years. For example, Senthil *et al.* proposed that a continuous quantum phase transition between the antiferromagnetic (AFM) order and the valence bond solid (VBS) order could exist [3,4], referred to as the deconfined quantum critical point (DQCP). Strong evidence of a DQCP in a spin-$\frac{1}{2}$ model on a square lattice has been first shown in the J-Q model by Sandvik [5,6]. Subsequently, other numerical examples and new theoretical understandings of the DQCP have been developed in quantum spin models [7–20] and have been gradually extended to interacting fermionic systems [21–27]. It is obvious that the model design and large-scale quantum Monte Carlo (QMC) simulations played a key role in pushing the frontier of our knowledge on such surprising phenomena.

Except for the DQCP discussed above, the interaction effects on massless Dirac fermions have also attracted great attention. Since the linear dispersion is stable against weak interactions, there must be one or more quantum phase transitions separating the Dirac semimetal (SM) phase and various possible Mott insulator states. Depending on the type of interactions, many Mott insulators have been discovered, including the ferromagnetic and AFM states [28–34], VBS state [35–40], nematic phase [41], superconductor and quantum (spin) Hall states [25–27,42,43], and many others. Among these examples, particular interest lies in the direction where from the Dirac SM to the strong-coupling limit, there exist multiple insulating phases as a function of the interaction strength, and leaves room for interesting intermediate phases such as topological ordered phases and multiple exotic quantum phase transitions, such as Gross-Neveu and DQCP. Previous works have shown, with spin-$\frac{1}{2}$ electron and SU(2) symmetry, an extended interaction on a honeycomb lattice offers a robust VBS with a Kekulé pattern exactly as such an intermediate phase between Dirac SM and strong-coupling AFM order [39]. However, although the transition between Dirac SM with a Kekulé VBS is found to be a Gross-Neveu QCP, the transition between VBS and AFM phases is first order. These results motivate us to investigate the interaction effect in a π-flux extended Hubbard model on a square lattice, as we show below, and in this case, except for a Gross-Neveu QCP between Dirac SM and VBS, there indeed further emerges a continuous transition between the VBS and AFM

*zymeng@hku.cn
†qiyang@fudan.edu.cn

 ©2022 American Physical Society

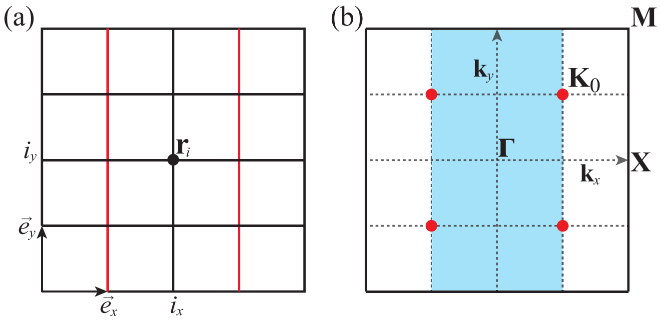

FIG. 1. (a) Square lattice with π-flux hopping. Red and black solid lines correspond to $-t$ and t. $\vec{e}_x$ ($\vec{e}_y$) is the unit vector along the x (y) direction. The position of site i is given as $\mathbf{r}_i = i_x\vec{e}_x + i_y\vec{e}_y$. (b) The white square is the BZ of the original square lattice, and the blue BZ is the folded one considering the translation-symmetry-breaking hopping amplitudes. The red solid points represent the position of Dirac cones $\mathbf{K}_0 = (\frac{\pi}{2}, \frac{\pi}{2})$. High-symmetry points $\mathbf{\Gamma} = (0, 0)$, $\mathbf{X} = (\pi, 0)$, and $\mathbf{M} = (\pi, \pi)$ are denoted.

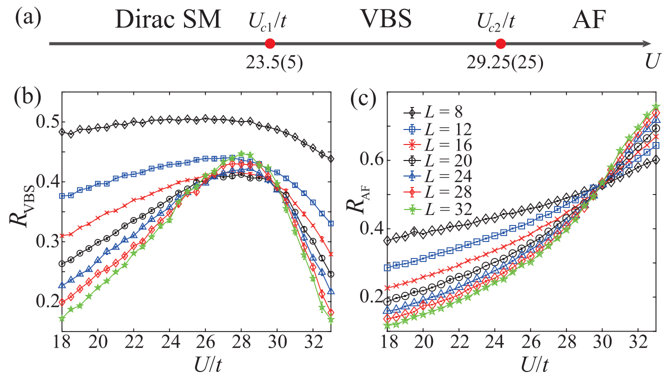

FIG. 2. (a) Phase diagram of the extended Hubbard model as a function of interaction strength U, obtained from QMC simulations. The SM-VBS transition at U_{c1} is continuous and of Gross-Neveu universality. The VBS-AFM transition at U_{c2} is also continuous and should be explained according to the deconfined quantum criticality. Correlation ratios of the (b) VBS order and (c) AFM order as a function of interaction strength U are shown

phase within the largest system sizes accessed, consistent with the expected behavior of the DQCP. Our results of the Dirac fermion with an extended interaction could also shed light on the great ongoing efforts in understanding the interaction effects on quantum moiré material models [40,44–50] such as twisted bilayer graphene (TBG) and transition metal dichalcogenides, where the interplay between flat-band Dirac cones and the extended Coulomb interactions can be engineered by twisting angles, and gating and tailored design of the dielectric environment, giving rise to a plethora of exotic phenomena.

II. MODEL AND METHOD

We study a SU(2) extended Hubbard model with a π-flux hopping term at half filling on a square lattice,

$$H = -\sum_{\langle ij\rangle,\sigma} t_{ij}(c^\dagger_{i\sigma}c_{j\sigma} + \text{H.c.}) + U\sum_{\square}(n_\square - 1)^2, \qquad (1)$$

where $\langle ij\rangle$ denotes the nearest neighbor, $c^\dagger_{i\sigma}$ and $c_{i\sigma}$ are creation and annihilation operators for fermions on site i with spin $\sigma = \uparrow, \downarrow$, $n_\square$ is the extended particle number operator of the $\square$ plaquette defined as $n_\square \equiv \frac{1}{4}\sum_{i\in\square} n_i$ with $n_i = \sum_\sigma c^\dagger_{i\sigma}c_{i\sigma}$ and at half filling $\langle n_\square\rangle = 1$, and U tunes the interaction strength, which favors AFM order in the strong-coupling limit [38].

As shown in Fig. 1(a), we set the hopping amplitudes $t_{i,i+\vec{e}_x} = t$ and $t_{i,i+\vec{e}_y} = (-1)^{i_x}t$, where the position of site i is given as $\mathbf{r}_i = i_x\vec{e}_x + i_y\vec{e}_y$ and $t = 1$ is the energy unit. Such an arrangement bestows a π flux penetrating each $\square$ plaqutte. As a consequence, two Dirac cones are located at $\mathbf{K}_0 = (\frac{\pi}{2}, \pm\frac{\pi}{2})$ in the first Brillouin zone (BZ). We note the folding and locations of the Dirac cones all depend on the gauge choice of hopping amplitudes, i.e., with the above hopping the BZ is folded in half [the blue area in Fig. 1(b)], but the distance between two Dirac cones is actually gauge invariant. The model therefore still has full crystalline symmetries of the square lattice (the $p4mm$ wallpaper group), where each crystalline symmetry operation is supplemented by a $U(1)$ gauge transformation. For example, the translation symmetry becomes $\hat{T}_{\vec{e}_x} : c_i \to (-1)^{i_y}c_{i+\vec{e}_x}$. Consequently, we will still discuss our results in the original square lattice BZ.

For the extended Hubbard interaction term, the on-site, first-, and second-nearest-neighbor repulsions are all included in one plaquette. This particular extended Coulomb interaction form can be related with quantum moiré materials with a square lattice structure. Because the Wannier orbitals of moiré materials, such as TBG, are quite extended, the relatively long-range Coulomb interactions have to be included to construct an effective model [51,52]. As found in previous studies [39,40,44,45], such an extended interaction will require a relative larger U to gap out the Dirac cones.

One can easily show the Hamiltonian in Eq. (1) is sign-problem free for auxiliary-field QMC [53] and we implement a projector version of the QMC method [54] to solve the model. Details of the algorithm can be found in the Supplemental Material (SM) [55], and we only mention the projection length $\beta t = L$ for equal-time measurements: $\beta t = L + 10$ for imaginary-time measurements and a discrete time slice $\Delta\tau = 0.1$. We simulate the systems with linear size $L = 12$, 16, 20, 24, 28, and 32. We have also tested that this setup is enough to achieve controlled error bars [55].

III. QMC RESULTS

The phase diagram obtained from QMC simulations is shown in Fig. 2(a). We find an emergent intermediate phase which realizes two continuous quantum phase transitions when gradually increasing the interaction strength U. They are the phase transitions from the Dirac SM to VBS phase and that from the VBS to AF phase. This particular sequence of transitions has yet to be observed in other models. The first corresponding QCP is at $U_{c1}/t = 23.5(5)$ and of Gross-Neveu type with the VBS acquiring a Z_4 discrete lattice symmetry breaking, and the critical point is expected to have emergent $U(1)$ symmetry as the Z_4 anisotropy is irrelevant [6]. The second corresponding QCP is at $U_{c2}/t = 29.25(25)$, separating two spontaneous symmetry-breaking phases, e.g., Z_4

for VBS and SU(2) for AFM phases, and shall be explained according to the deconfined quantum criticality [3,4]. What is more, the corresponding critical exponents $\eta_{\mathrm{VBS}} = 0.6(1)$ and $\eta_{\mathrm{AFM}} = 0.58(3)$ are extracted, and they satisfy the CFT bootstrap bound [56,57]. In particular, our model is a one-tuning-parameter fermionic model that gives rise to the critical exponents $\eta_{\mathrm{VBS}} \approx \eta_{\mathrm{AFM}}$ meeting the CFT bootstrap bound at DQCP.

To quantitatively study the two phase transitions, we define two structure factors,

$$C_{\mathrm{AFM}}(\mathbf{k}, L) = \frac{1}{L^4} \sum_{i,j} e^{i\mathbf{k}\cdot(\mathbf{r}_i - \mathbf{r}_j)} \langle \mathbf{S}_i \mathbf{S}_j \rangle \tag{2}$$

and

$$C_{\mathrm{VBS}}(\mathbf{k}, L) = \frac{1}{L^4} \sum_{i,j} e^{i\mathbf{k}\cdot(\mathbf{r}_i - \mathbf{r}_j)} \langle B_i B_j \rangle, \tag{3}$$

for AFM order and VBS order, respectively. In the above equations, $\mathbf{S}_i = \frac{1}{2}\sum_{\sigma\sigma'} c^{\dagger}_{i\sigma} \boldsymbol{\sigma}_{\sigma\sigma'} c_{i\sigma'}$ are the fermion spin operators at site i, and $\boldsymbol{\sigma}$ the Pauli matrices. Here, $B_i = \sum_{\sigma}(t_{i,i+\vec{e}_x} c^{\dagger}_{i,\sigma} c_{i+\vec{e}_x,\sigma} + \mathrm{H.c.})$ are gauge invariant bond operators. For AFM order, $C_{\mathrm{AFM}}(\mathbf{k}, L)$ is peaked at momentum $\mathbf{M} = (\pi, \pi)$; for VBS order, $C_{\mathrm{VBS}}(\mathbf{k}, L)$ is peaked at momentum $\mathbf{X} = (\pi, 0)$. We then use the renormalization-group invariant correlation ratios ($c = $ VBS, AFM) to perform the data analysis,

$$R_c(U, L) = 1 - \frac{C_c(\mathbf{k} = \mathbf{Q} + d\mathbf{q}, L)}{C_c(\mathbf{k} = \mathbf{Q}, L)}, \tag{4}$$

where $\mathbf{Q}$ is the ordering wave vector, and $|d\mathbf{q}| \sim \frac{1}{L}$ denotes the smallest momentum on finite-size lattice. By definition, $R_c(U, L) \to 1$ (0) for $L \to \infty$ in the corresponding ordered (disordered) phase. At the QCP, R_c is scale invariant for sufficiently large L and exhibits the scaling behavior for the corresponding universalities [23,32,58–60].

As shown in Fig. 2(b), when varying U/t from 18 to 33, $R_{\mathrm{VBS}}(U, L)$ first increases then decreases. Importantly, $R_{\mathrm{VBS}}(U, L = 20, 24, 28, 32)$ for different L's cross at two separate regions. These results mean that our model undergoes two phase transitions, and the VBS order is the intermediate phase. Admittedly, the VBS order is very weak but remains finite at the thermodynamic limit (TDL), and we believe it is attributed to the enhanced quantum fluctuations from the interplay of Dirac fermions and extended interactions within a plaquette. We also find that at the transition, the VBS order parameter histogram is consistent with the emergent $U(1)$ symmetry [39]. The correlation ratio of AFM order is shown in Fig. 2(c). Interestingly, a clear crossing takes place around $U/t = 29.4$, which further indicates the phase transition between the VBS and the AFM order is continuous.

To understand the two intriguing QCPs, we first focus on the more complicated VBS-AFM transition, to demonstrate it has the flavor of DQCP. To this end, we collapse the correlation ratio of AFM order with the finite-size scaling relation $R_{\mathrm{AF}}(U, L) = f_1[L^{1/\nu}(U/U_c - 1)]$, as shown in Fig. 3(a), and obtain the position of the corresponding QCP at $U_{c2}/t = 29.25(25)$ and the correlation length exponent $\nu = 1.13(5)$. Then at U_{c2} the AFM and VBS structure factors, in Eqs. (2) and (3), shall obey the following finite-size scaling ansatz

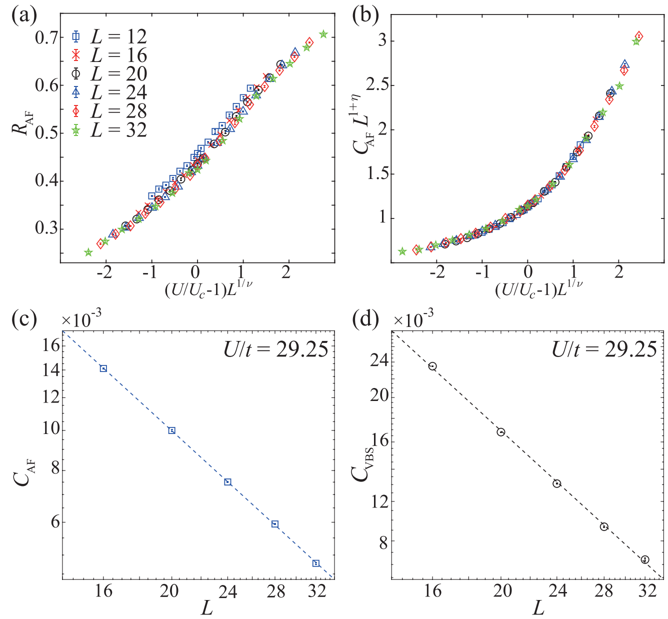

FIG. 3. (a) The data collapse of the correlation ratio R_{AFM}, which gives $U_{c2}/t = 29.25(25)$ and $\nu = 1.13(5)$. (b) The data collapse of the AFM structure in the vicinity of $U_{c2}/t = 29.25$ with $\nu = 1.13$ and $\eta = 0.58$. The log-log plot of the structure factor of (c) AFM order and (d) VBS order vs the linear lattice size L at $U_{c2}/t = 29.25$. The critical exponents $1 + \eta$ can be extracted from the slopes of linear fitting curves in log-log plots. We obtain $\eta_{\mathrm{AFM}} = 0.58(3)$ and $\eta_{\mathrm{VBS}} = 0.6(1)$.

[40,61],

$$C_c(U, L) = L^{-z-\eta} f_2[L^{1/\nu}(U - U_c)/U_c], \tag{5}$$

where η is the anomalous dimension exponent, and $z = 1$ is the dynamic exponent. As shown in Figs. 3(c) and 3(d), we extract η from the slope of the log-log plot of $C_c(U, L)$ curves at $U_{c2}/t = 29.25$ and find $\eta_{\mathrm{AFM}} = 0.58(3)$ for AFM order and $\eta_{\mathrm{VBS}} = 0.6(1)$ for VBS order, respectively, giving rise to good quality linear fits.

According to the scenario of DQCP [3,4], the closeness of the exponents from the two ordered phases approaching the critical point, i.e., $\eta_{\mathrm{VBS}} \approx \eta_{\mathrm{AFM}}$ in our setting, is considered as an important signature for the associated emergent symmetry [8,9], and numerical evidence of such closenesses has been seen in the J-Q model [5,12], the three-dimensional (3D) loop model [9], as well as those in the recently discovered fermionic models [23,25–27]. In the literature [8,9,12,23,25–27], the precise value of the exponents appears to depend on the detailed implementation of each model, and there also exists the conformal field theory (CFT) bound that the emergent symmetry needs to satisfy [56,57]. We note the η_{VBS} and η_{AFM} in our work satisfy the CFT bootstrap bound, as well as in a completely different interacting fermion model on a honeycomb lattice in Ref. [23]. Importantly, comparing with Ref. [23], we only use one tuning parameter in our model, as there is no interference from the nearby multicriticality or first-order transition as in Ref. [23], which may pollute the measurement of critical exponents because a clean scaling behavior can only be observed far away from the multicritical

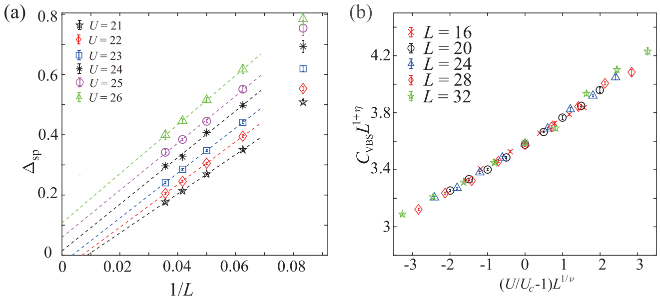

FIG. 4. (a) The $1/L$ extrapolation of the single-particle gap $\Delta_{sp}(\mathbf{K}_0, L)$: The gap opens at an interaction strength locating in a range from $U/t = 23$ to $U/t = 24$. (b) The data collapse of the structure factor of VBS order, which gives an estimation of $U_{c1}/t = 23.5(5)$, $\nu' = 1.0(1)$, and $\eta' = 0.89(3)$.

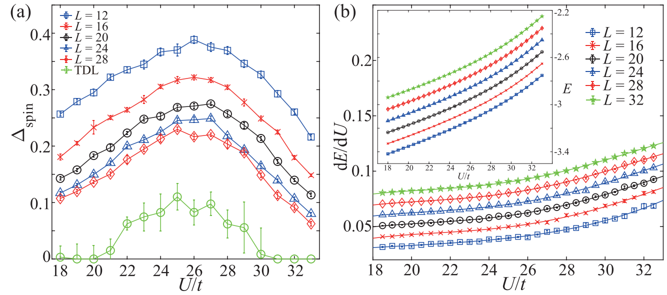

FIG. 5. (a) Spin excitation gap $\Delta_{sp}(\mathbf{K}_0)$ for different L's and their TDL extrapolation as a function of interaction strength U. The VBS phase has a finite spin gap due to the formation of singlets. (b) Main panel: First derivative of kinetic energy density as a function of U. The solid curves are a cubic polynomial fitting through the data. No discontinuity observed. Inset: Kinetic energy density as a function of U. Lines and points in both the main panel and inset are shifted for visualization purposes without changing the physical meaning. Error bars are smaller than the symbols.

point or first-order transitions. The more recent entanglement measurements further point out the DQCP, at least in the J-Q model, might not be a unitary CFT in the first place [18,20] and other possible scenarios such as multicritical points [16], complex CFT [62,63], and weakly first-order transitions [17] have been constantly and actively proposed and explored. Despite these efforts and the enigmatic situation of the DQCP, our observation, that within the system sizes simulated $\eta_{\text{VBS}} \approx \eta_{\text{AFM}}$, is consistent with the deconfinement at U_{c2}. It is further worthwhile to point out that a relatively large $\eta \sim 0.6$ is also the hallmark of many QCPs associated with the fractionalization of elementary excitations such as the condensation transition of spinons and visons in Z_N topological orders [64–66]. We also collapse the AFM structure factor according to Eq. (5) with $U_{c2}/t = 29.25$, $\nu = 1.13$, and $\eta = 0.58$, and as shown in Fig. 3(b), all data points fall on a smooth curve. Therefore, our numerical data in Fig. 3 certainly reveal an internally consistent description along the line of DQCP for the VBS-AFM transition.

Next, we move on to the SM-VBS transition. It is known that the massless Dirac fermion is robust at weak interaction, and a single-particle gap will open at a finite interaction strength [24,44]. In our model, we indeed find that as a function of U, the Dirac SM transits to an insulating VBS order continuously through a Gross-Neveu QCP [22,37,39,40,61,67–76]. This is also consistent with a similar situation of the extended Hubbard model on a honeycomb lattice [39,40].

To determine U_{c1}, we extract the single-particle gap $\Delta_{sp}(\mathbf{K}_0, L)$ from a fit to the asymptotic long imaginary-time behavior of the single-particle Green's function $G(\mathbf{k}, \tau, L) = (1/L^4)\sum_{i,j,\sigma} e^{i\mathbf{k}\cdot(\mathbf{r}_i-\mathbf{r}_j)}\langle c^\dagger_{i,\sigma}(\tau)c_{j,\sigma}(0)\rangle \propto e^{-\Delta_{sp}(\mathbf{k},L)\tau}$. The obtained $\Delta_{sp}(\mathbf{K}_0, L)$ are shown in Fig. 4(a). It is clear that $\Delta_{sp}(\mathbf{K}_0, L \to \infty) \to 0$ at $U/t < 23$ and $\Delta_{sp}(\mathbf{K}_0, L \to \infty) > 0$ at $U/t > 24$, which indicates $U_{c1}/t \in (23, 24)$ and is overall consistent with the cross point of R_{VBS} shown in Fig. 2(b). This again signifies the weakness of the VBS order and the strong fluctuations at this QCP which give rise to a strong finite-size effect. To locate the U_{c1} more accurately, as shown in Fig. 4(b), we collapse the VBS structure factor according to Eq. (5) in $U/t \in (23, 24)$. Although the finite-size effect is strong, the data collapse nevertheless gives rise to an estimation, $U_{c1}/t = 23.5(5)$, and critical exponents, $\nu' = 1.0(1)$ and $\eta' = 0.89(3)$. These exponents are consistent with previous numerical simulations of similar SM-VBS transitions on the honeycomb lattice [39], where it is found that the threefold lattice rotation symmetry is enhanced to an emergent $U(1)$ at the Gross-Neveu QCP. Since the threefold anisotropy of the $U(1)$ order parameter is (dangerously) irrelevant at the QCP, it is expected that the fourfold anisotropy should be even more irrelevant in our case.

At $U < U_{c1}$, the ground state is in a Dirac SM state, and thus there is no spin excitation gap in the TDL. At $U > U_{c2}$, the ground state is in an AFM state, and the spin excitation gap in the TDL should also vanish because of the existence of the Goldstone mode. However, the spin excitation gap will open in the VBS state due to the formation of a spin singlet [40]. To verify the theoretical predictions, we measure the dynamical spin-spin correlation function $C(\mathbf{k}, \tau, L) = \frac{1}{L^4}\sum_{i,j} e^{i\mathbf{k}\cdot(\mathbf{r}_i-\mathbf{r}_j)}\langle \mathbf{S}_i(\tau)\mathbf{S}_j(0)\rangle$. The spin excitation gap $\Delta_{\text{spin}}(\mathbf{M}, L)$ can be extract from the imaginary-time decay of $C(\mathbf{k}, \tau, L) \propto e^{-\Delta_{\text{spin}}(\mathbf{k},L)\tau}$. As shown in Fig. 5(a) we extrapolate the spin excitation gap to the TDL and find that $\Delta_{\text{spin}}(\mathbf{M})$ goes to a finite value near U_{c1} and goes back to zero near U_{c2}. These QMC results are consistent with our above theoretical analysis, and thus confirm the process of the evolution of the ground state of our model, i.e., transiting from the Dirac SM to VBS state first and then from the VBS to AFM state, as a function of interaction strength U.

In addition, we provide more evidence that the two QCPs are continuous within the system size studied, by means of monitoring the evolution of the expectation value of the kinetic energy density. Since our QMC is of projector type, this is meant to monitor the evolution of the (part of) the free energy of the system. As shown in the inset of Fig. 5(b), the kinetic energy density $E = \frac{1}{L^4}\langle -\sum_{\langle ij\rangle,\sigma} t_{ij}(c^\dagger_{i\sigma}c_{j\sigma} + \text{H.c.})\rangle$ evolves smoothly as a function of U for different system sizes. We then compute their first-order derivatives and find in the main panel of Fig. 5(b) no discontinuities, consistent with the continuous phase transition. In the SM [55], we also present a similar analysis of the structure factors for AFM and

VBS orders. They support the notion that the SM-VBS and VBS-AFM transitions are all continuous.

IV. DISCUSSIONS

With the help of a large-scale sign-free projector QMC simulation, we investigate the phase diagram of a π-flux extended Hubbard model on a square lattice at half filling. Based on all the numerical results obtained, we conclude that this simple looking model acquires an interesting phase diagram with an intermediate phase with weak VBS order separating the well-known Dirac SM and AFM phases. More importantly, we find the Gross-Neveu transition from the Dirac SM to VBS is continuous, and the transition from VBS to AFM is also continuous, consistent with deconfined quantum critical criticality.

Our results, along with the previous works of an extended interaction model on a honeycomb lattice [38–40], point out the directions that to realize interesting phase diagrams with (multiple) intermediate phases between the free Dirac SM and strong-coupling Mott insulators, the extended interactions beyond the on-site Hubbard term are crucial and could bring more surprises. In fact, the weak VBS order discovered here and the DQCP associated with it towards the AFM order, imply further perturbations could give rise to even more exotic interaction-driven phases and transitions. In this context, our results also have relevance to the great ongoing efforts in understanding the interaction effect on quantum moiré material models [38–40,44–48] such as twisted bilayer graphene and transition metal dichalcogenides, where the interplay between flat-band Dirac cones and the extended Coulomb interactions can be engineered by twisting angles, and gating and tailored design of the dielectric environment, giving rise to a plethora of exotic phenomena and interesting phase and phase transitions. It is natural to anticipate, with the technique and analysis presented in this work, once further degrees of freedom and tunabilities in moiré systems are added, interesting phases and transitions and their mechanism will be revealed from the lattice model simulations.

Note added. Recently, we become aware of a related investigation by Zhu *et al.* [77], in which consistent results are obtained.

ACKNOWLEDGMENTS

Y.D.L. acknowledges the support of a project funded by China Postdoctoral Science Foundation through Grants No. 2021M700857 and No. 2021TQ0076. X.Y.X. is sponsored by the National Key R&D Program of China (Grant No. 2021YFA1401400), Shanghai Pujiang Program under Grant No. 21PJ1407200, Yangyang Development Fund, and startup funds from SJTU. Z.Y.M. acknowledges support from the Research Grants Council of Hong Kong SAR of China (Grants No. 17303019, No. 17301420, No. 17301721, and No. AoE/P-701/20), the GD-NSF (No. 2022A1515011007), the K. C. Wong Education Foundation (Grant No. GJTD-2020-01), and the Seed Funding "Quantum-Inspired explainable-AI" at the HKUTCL Joint Research Centre for Artificial Intelligence. Y.Q. acknowledges support from the National Natural Science Foundation of China (Grants No. 11874115 and No. 12174068). The authors also acknowledge Beijng PARATERA Tech Co., Ltd. [78] for providing HPC resources that have contributed to the research results reported within this paper.

[1] L. D. Landau, E. M. Lifshitz, and E. M. Pitaevskii, *Statistical Physics* (Elsevier, Amsterdam, 1980).
[2] K. G. Wilson and J. Kogut, Phys. Rep. **12**, 75 (1974).
[3] T. Senthil, A. Vishwanath, L. Balents, S. Sachdev, and M. P. A. Fisher, Science **303**, 1490 (2004).
[4] T. Senthil, L. Balents, S. Sachdev, A. Vishwanath, and M. P. A. Fisher, Phys. Rev. B **70**, 144407 (2004).
[5] A. W. Sandvik, Phys. Rev. Lett. **98**, 227202 (2007).
[6] J. Lou, A. W. Sandvik, and N. Kawashima, Phys. Rev. B **80**, 180414(R) (2009).
[7] M. S. Block, R. G. Melko, and R. K. Kaul, Phys. Rev. Lett. **111**, 137202 (2013).
[8] A. Nahum, P. Serna, J. T. Chalker, M. Ortuño, and A. M. Somoza, Phys. Rev. Lett. **115**, 267203 (2015).
[9] A. Nahum, J. T. Chalker, P. Serna, M. Ortuño, and A. M. Somoza, Phys. Rev. X **5**, 041048 (2015).
[10] L. Wang, Z.-C. Gu, F. Verstraete, and X.-G. Wen, Phys. Rev. B **94**, 075143 (2016).
[11] H. Shao, W. Guo, and A. W. Sandvik, Science **352**, 213 (2016).
[12] Y. Q. Qin, Y.-Y. He, Y.-Z. You, Z.-Y. Lu, A. Sen, A. W. Sandvik, C. Xu, and Z. Y. Meng, Phys. Rev. X **7**, 031052 (2017).
[13] J. D'Emidio and R. K. Kaul, Phys. Rev. Lett. **118**, 187202 (2017).
[14] N. Ma, G.-Y. Sun, Y.-Z. You, C. Xu, A. Vishwanath, A. W. Sandvik, and Z. Y. Meng, Phys. Rev. B **98**, 174421 (2018).
[15] N. Ma, Y.-Z. You, and Z. Y. Meng, Phys. Rev. Lett. **122**, 175701 (2019).
[16] B. Zhao, J. Takahashi, and A. W. Sandvik, Phys. Rev. Lett. **125**, 257204 (2020).
[17] J. D'Emidio, A. A. Eberharter, and A. M. Läuchli, arXiv:2106.15462.
[18] Y.-C. Wang, N. Ma, M. Cheng, and Z. Y. Meng, arXiv:2106.01380.
[19] Y.-R. Shu, S.-K. Jian, and S. Yin, Phys. Rev. Lett. **128**, 020601 (2022).
[20] J. Zhao, Y.-C. Wang, Z. Yan, M. Cheng, and Z. Y. Meng, Phys. Rev. Lett. **128**, 010601 (2022).
[21] T. Sato, M. Hohenadler, and F. F. Assaad, Phys. Rev. Lett. **119**, 197203 (2017).
[22] Z.-X. Li, Y.-F. Jiang, S.-K. Jian, and H. Yao, Nat. Commun. **8**, 314 (2017).
[23] Z.-X. Li, S.-K. Jian, and H. Yao, arXiv:1904.10975.
[24] Z. H. Liu, M. Vojta, F. F. Assaad, and L. Janssen, Phys. Rev. Lett. **128**, 087201 (2022).
[25] Y. Liu, Z. Wang, T. Sato, M. Hohenadler, C. Wang, W. Guo, and F. F. Assaad, Nat. Commun. **10**, 2658 (2019).
[26] Z. Wang, M. P. Zaletel, R. S. K. Mong, and F. F. Assaad, Phys. Rev. Lett. **126**, 045701 (2021).
[27] Z. Wang, Y. Liu, T. Sato, M. Hohenadler, C. Wang, W. Guo, and F. F. Assaad, Phys. Rev. Lett. **126**, 205701 (2021).

[28] Z. Y. Meng, T. C. Lang, S. Wessel, F. F. Assaad, and A. Muramatsu, Nature (London) **464**, 847 (2010).
[29] C.-C. Chang and R. T. Scalettar, Phys. Rev. Lett. **109**, 026404 (2012).
[30] Y. Otsuka, S. Yunoki, and S. Sorella, Phys. Rev. X **6**, 011029 (2016).
[31] F. Parisen Toldin, M. Hohenadler, F. F. Assaad, and I. F. Herbut, Phys. Rev. B **91**, 165108 (2015).
[32] T. C. Lang and A. M. Läuchli, Phys. Rev. Lett. **123**, 137602 (2019).
[33] X. Y. Xu and T. Grover, Phys. Rev. Lett. **126**, 217002 (2021).
[34] S. M. Tabatabaei, A.-R. Negari, J. Maciejko, and A. Vaezi, Phys. Rev. Lett. **128**, 225701 (2022).
[35] F. F. Assaad, Phys. Rev. B **71**, 075103 (2005).
[36] T. C. Lang, Z. Y. Meng, A. Muramatsu, S. Wessel, and F. F. Assaad, Phys. Rev. Lett. **111**, 066401 (2013).
[37] Z. Zhou, D. Wang, Z. Y. Meng, Y. Wang, and C. Wu, Phys. Rev. B **93**, 245157 (2016).
[38] Y. Ouyang and X. Y. Xu, Phys. Rev. B **104**, L241104 (2021).
[39] X. Y. Xu, K. T. Law, and P. A. Lee, Phys. Rev. B **98**, 121406(R) (2018).
[40] Y. Da Liao, Z. Y. Meng, and X. Y. Xu, Phys. Rev. Lett. **123**, 157601 (2019).
[41] J. Schwab, L. Janssen, K. Sun, Z. Y. Meng, I. F. Herbut, M. Vojta, and F. F. Assaad, Phys. Rev. Lett. **128**, 157203 (2022).
[42] X. Y. Xu, K. S. D. Beach, K. Sun, F. F. Assaad, and Z. Y. Meng, Phys. Rev. B **95**, 085110 (2017).
[43] Y.-Y. He, X. Y. Xu, K. Sun, F. F. Assaad, Z. Y. Meng, and Z.-Y. Lu, Phys. Rev. B **97**, 081110(R) (2018).
[44] Y.-D. Liao, X.-Y. Xu, Z.-Y. Meng, and J. Kang, Chin. Phys. B **30**, 017305 (2021).
[45] Y. D. Liao, J. Kang, C. N. Breiø, X. Y. Xu, H.-Q. Wu, B. M. Andersen, R. M. Fernandes, and Z. Y. Meng, Phys. Rev. X **11**, 011014 (2021).
[46] X. Zhang, G. Pan, Y. Zhang, J. Kang, and Z. Y. Meng, Chin. Phys. Lett. **38**, 077305 (2021).
[47] G. Pan, X. Zhang, H. Li, K. Sun, and Z. Y. Meng, Phys. Rev. B **105**, L121110 (2022).
[48] X. Zhang, K. Sun, H. Li, G. Pan, and Z. Y. Meng, arXiv:2111.10018.
[49] B.-B. Chen, Y. D. Liao, Z. Chen, O. Vafek, J. Kang, W. Li, and Z. Y. Meng, Nat. Commun. **12**, 5480 (2021).
[50] X. Lin, B.-B. Chen, W. Li, Z. Y. Meng, and T. Shi, Phys. Rev. Lett. **128**, 157201 (2022).
[51] M. Koshino, N. F. Q. Yuan, T. Koretsune, M. Ochi, K. Kuroki, and L. Fu, Phys. Rev. X **8**, 031087 (2018).
[52] H. C. Po, L. Zou, A. Vishwanath, and T. Senthil, Phys. Rev. X **8**, 031089 (2018).
[53] C. Wu and S.-C. Zhang, Phys. Rev. B **71**, 155115 (2005).
[54] F. Assaad and H. Evertz, in *Computational Many-Particle Physics*, edited by H. Fehske, R. Schneider, and A. Weiße, Lecture Notes in Physics Vol. 739 (Springer, Berlin, 2008), pp. 277–356.
[55] See Supplemental Material at http://link.aps.org/supplemental/10.1103/PhysRevB.106.075111 for the implementation of the projector quantum Monte Carlo simulation, the analysis of the Trotter error, and more data of structure factors as a function of interaction strength.
[56] Y. Nakayama and T. Ohtsuki, Phys. Rev. Lett. **117**, 131601 (2016).
[57] D. Poland, S. Rychkov, and A. Vichi, Rev. Mod. Phys. **91**, 015002 (2019).
[58] M. Campostrini, A. Pelissetto, and E. Vicari, Phys. Rev. B **89**, 094516 (2014).
[59] R. K. Kaul, Phys. Rev. Lett. **115**, 157202 (2015).
[60] S. Pujari, T. C. Lang, G. Murthy, and R. K. Kaul, Phys. Rev. Lett. **117**, 086404 (2016).
[61] Z. Zhou, C. Wu, and Y. Wang, Phys. Rev. B **97**, 195122 (2018).
[62] R. Ma and C. Wang, Phys. Rev. B **102**, 020407(R) (2020).
[63] A. Nahum, Phys. Rev. B **102**, 201116(R) (2020).
[64] S. V. Isakov, R. G. Melko, and M. B. Hastings, Science **335**, 193 (2012).
[65] Y.-C. Wang, X.-F. Zhang, F. Pollmann, M. Cheng, and Z. Y. Meng, Phys. Rev. Lett. **121**, 057202 (2018).
[66] Y.-C. Wang, M. Cheng, W. Witczak-Krempa, and Z. Y. Meng, Nat. Commun. **12**, 5347 (2021).
[67] D. J. Gross and A. Neveu, Phys. Rev. D **10**, 3235 (1974).
[68] S. Hands, A. Kocic, and J. Kogut, Ann. Phys. **224**, 29 (1993).
[69] B. Rosenstein, H.-L. Yu, and A. Kovner, Phys. Lett. B **314**, 381 (1993).
[70] N. Zerf, L. N. Mihaila, P. Marquard, I. F. Herbut, and M. M. Scherer, Phys. Rev. D **96**, 096010 (2017).
[71] M. M. Scherer and I. F. Herbut, Phys. Rev. B **94**, 205136 (2016).
[72] L. N. Mihaila, N. Zerf, B. Ihrig, I. F. Herbut, and M. M. Scherer, Phys. Rev. B **96**, 165133 (2017).
[73] S.-K. Jian and H. Yao, Phys. Rev. B **96**, 195162 (2017).
[74] L. Classen, I. F. Herbut, and M. M. Scherer, Phys. Rev. B **96**, 115132 (2017).
[75] E. Torres, L. Classen, I. F. Herbut, and M. M. Scherer, Phys. Rev. B **97**, 125137 (2018).
[76] B. Ihrig, L. N. Mihaila, and M. M. Scherer, Phys. Rev. B **98**, 125109 (2018).
[77] X. Zhu, Y. Huang, H. Guo, and S. Feng, arXiv:2204.12147.
[78] https://www.paratera.com/.